Analytical and Bioanalytical Chemistry (2022) 414:623–637
https://doi.org/10.1007/s00216-021-03570-7

RESEARCH PAPER

Utilizing liquid chromatography, ion mobility spectrometry, and mass spectrometry to assess INLIGHT™ derivatized *N*-linked glycans in biological samples

Karen E. Butler[1] · Jaclyn Gowen Kalmar[1] · David C. Muddiman[1,2,3] · Erin S. Baker[1,2,4]

Received: 15 May 2021 / Revised: 6 July 2021 / Accepted: 20 July 2021 / Published online: 4 August 2021

Abstract

Glycosylation is a ubiquitous co- and post-translational modification involved in the sorting, folding, and trafficking of proteins in biological systems; in humans, >50% of gene products are glycosylated with the cellular machinery of glycosylation compromising ~2% of the genome. Perturbations in glycosylation have been implicated in a variety of diseases including neurodegenerative diseases and certain types of cancer. However, understanding the relationship between a glycan and its biological role is often difficult due to the numerous glycan isomers that exist. To address this challenge, nanoflow liquid chromatography, ion mobility spectrometry, and mass spectrometry (nLC-IMS-MS) were combined with the Individuality Normalization when Labeling with the Isotopic Glycan Hydrazide Tags (INLIGHT™) strategy to study a series of glycan standards and those enzymatically released from the glycoproteins horseradish peroxidase, fetuin, and pooled human plasma. The combination of IMS and the natural (NAT) and stable-isotope label (SIL) in the INLIGHT™ strategy provided additional confidence for each glycan identification due to the mobility aligned NAT- and SIL-labeled glycans and further capabilities for isomer examinations. Additionally, molecular trend lines based on the IMS and MS dimensions were investigated for the INLIGHT™ derivatized glycans, facilitating rapid identification of putative glycans in complex biological samples.

Keywords Glycomics · Ion mobility spectrometry · INLIGHT™ · *N*-Linked glycans · LC-IMS-MS

Introduction

Glycosylation, or the affixing of carbohydrate moieties to proteins, is a co- and post-translational modification linked to host-pathogen interactions [1], immune system response [2], and protein folding, sorting, and stability within eukaryotic systems [3, 4]. While glycans can be either *N*- or *O*-linked, to date, *N*-linked are the most commonly studied due to their specific locations and conserved core structure [5]. For example, *N*-linked glycans are commonly affixed to the sequon N-X-S/T, where N is asparagine, S/T is either serine or threonine, and X is any amino acid except for proline. Since up to 70% of proteins are estimated to contain this sequon, *N*-linked glycosylation is thought to be highly prevalent in eukaryotic systems [6]. Their common core structure allows them to be targeted and readily cleaved using the enzyme peptide *N*-glycosidase F (PNGase F), making their study easier than that of *O*-linked glycans which have a variable structure [7]. However, *N*-linked glycans follow a non-template-driven synthesis, resulting in a highly heterogeneous class of molecules [7]. The manner in which the individual monosaccharides in *N*-linked glycans are linked to one another is also variable, either through α or β linkages, contributing to the enormous complexity of this molecular class. As glycosylation has been

Published in the topical collection celebrating *ABCs 20th Anniversary*.

✉ Erin S. Baker
ebaker@ncsu.edu

[1] Department of Chemistry, North Carolina State University, Raleigh, NC 27695, USA

[2] Center for Human Health and the Environment, North Carolina State University, Raleigh, NC 27695, USA

[3] Molecular Education, Technology, and Research Innovation Center (METRIC), North Carolina State University, Raleigh, NC 27695, USA

[4] Comparative Medicine Institute, North Carolina State University, Raleigh, NC 27695, USA

implicated in the onset and progression of multiple diseases and even COVID-19 [8–11], studies are needed to better define the precise structures of both *N*- and *O*-linked glycans and ultimately relate them to function.

Efforts towards elucidating the relationship between glycan structure and function have primarily been hampered by the lack of analytical tools capable of characterizing the glycosidic linkages and individual monosaccharides. Mass spectrometry (MS) has become a preferred method for the analysis of glycans, as it requires a small quantity of sample, is readily coupled with chromatographic separation, and yields structural information using different fragmentation strategies. However, fragmentation information alone is often insufficient for complete characterization of glycan structure given the large number of isomeric monosaccharides and diversity of glycosidic linkages [12]. Thus, it is often through a combination of liquid chromatography (LC) separations, MS fragmentation data, and knowledge of biosynthetic pathways that glycan structures are predicted [13]. Analysis of glycans using LC is challenging as they are exceedingly hydrophilic molecules which precludes LC separation with reversed-phase LC (RPLC) without derivatization. Therefore, hydrophilic interaction liquid chromatography (HILIC) and porous graphitic carbon (PGC) are popular options for glycan LC separations [14, 15].

The hydrophilicity of glycans also complicates MS analyses when using an electrospray ionization (ESI) source, as ESI is inherently biased towards hydrophobic analytes [16, 17]. To overcome this challenge, several types of derivatization chemistry have been employed to increase the overall hydrophobicity of *N*-linked glycans and improve their detection in both MS and spectroscopic methods. One of the more commonly employed derivatization approaches is permethylation. In permethylation, the hydroxyl, amino, and carboxylic acid groups located on the glycan structure are chemically modified to their corresponding methyl-ether [18–20]. This significantly increases the non-polar surface area (NPSA) of the molecule, resulting in an increase in hydrophobicity that facilitates RPLC and increases ESI abundances. Alternatively, the use of derivatization reagents with a reductive amination mechanism, such as 2-aminobenzoic acid (2-AA) and 2-aminobenzamide (2-AB), also enhances *N*-linked glycans using both MS and spectroscopic means [21]. Oxime formation by means of aminooxy reagents, such as Tandem Mass Tags (TMT)™[22], or derivatization methods that use hydrozone formation [23, 24] have also become an attractive option for labeling glycans. While all derivation strategies enhance the number of glycans observed by MS, the unpredictability of inefficient derivatization complicates the identifications in complex biological samples and hinders quantification. Most of these methods also require time-consuming clean-up steps, decreasing throughput.

The Individuality Normalization when Labeling with Isotopic Glycan Hydrizide Tags (INLIGHT™) strategy is a derivatization method previously used to examine *N*-linked glycans in complex biological samples [25]. In this strategy, *N*-linked glycans enzymatically released from glycoproteins by PNGase F are derivatized using hydrazide chemistry at the reducing GlcNAc residue with either natural (NAT) or stable-isotope ($^{13}C_6$) label (SIL) 4-phenethylbenzohydrazide (P2GPN) reagent [23, 25, 26]. This reagent has 95% derivatization efficiency and also increases the glycan's nonpolar surface area (NPSA) [23]. The use of both a NAT and $^{13}C_6$ incorporated SIL in INLIGHT™ enables the relative quantification of *N*-linked glycans in complex biological samples as the NAT and SIL INLIGHT™ tags have an exact mass difference of 6.0201 Da [25]. Additionally, the use of $^{13}C_6$ prevents overlapping isotopic distributions, which may skew quantitative assessments [23–25] and allows for LC co-elution of the NAT and SIL glycans [17, 24, 25, 27]. Furthermore, this derivatization method does not require significant sample clean-up and has been demonstrated to work well within a filter-aided *N*-glycan sample (FANGS) preparation strategy [26].

Due to its ability to distinguish isomeric molecules, ion mobility spectrometry-mass spectrometry (IMS-MS) has previously been explored to investigate the structure and function of glycans in biological systems [28, 29]. The IMS-MS investigations have shown discrimination of glycan and glycopeptide epimers [30] in samples ranging from simple systems such as standards and glycans enzymatically released from glycoproteins [31] to complex applications in patients with liver cancer and cirrhosis [32]. These studies and the ability of IMS-MS to resolve native isomeric glycans have expanded our knowledge of glycan structural diversity [33–35]. IMS-MS has also been applied to the analysis of derivatized *N*-linked glycans [31, 36, 37]. Specifically, the study of permethylated glycans and glycopeptides by Glaskin et al. resulted in a CCS database for permethylated *N*-linked glycans from several commonly used glycoprotein standards, including bovine fetuin and α-1-acid glycoprotein [36].

Herein, we present the first application of drift tube IMS (DTIMS)-MS to *N*-linked glycans derivatized using the INLIGHT™ strategy. The collision cross-section (CCS) values determined with DTIMS relate directly to the size of the molecule and enabled a deeper characterization of the glycans in addition to their LC retention times, *m*/*z* values, and fragmentation patterns [38, 39]. Furthermore, since the incorporation of ^{13}C does not significantly alter the shape of the glycans, rapid identification and relative quantification of putative glycans in complex biological samples are possible by both their distinctive isotopic distribution and the drift time alignment of the NAT and SIL derivatized glycans. In this work, nLC-IMS-MS was combined with the INLIGHT™ strategy to assess a series of glycan standards and those enzymatically released from the glycoproteins horseradish peroxidase, fetuin, and pooled human plasma and the identification, quantification, and trends are reported.

Materials and methods

Materials Maltoheptaose (≥ 60%, HPLC), 7 glycan standards ($(GlcNAc)_2Man_5$, $(Neu5Ac\text{-}Gal\text{-}GlcNAc)_3Man_3(GlcNAc)_2$, $(Gal\text{-}GlcNAc)_2Man_3(GlcNAc)_2$, $(GlcNAc)_2Man_9$, $(Neu5Ac\text{-}Gal\text{-}GlcNAc)_2Man_3(Fuc)(GlcNAc)_2$, $GalGlcNAc_2Man_3GlcNAc_2$glycan, and $(GlcNAc)_2Man_3(Fuc)(GlcNAc)_2$ glycan), and 2 glycoprotein standards (horseradish peroxidase and fetuin), as well as ammonium bicarbonate, iodoacetamide, and dithiothreitol (DTT), were purchased from Sigma Aldrich (St. Louis, MO). Human plasma (K2 EDTA, male and female) used in this study was obtained from Golden West Biologicals (Temecula, CA). INLIGHT™ P2GPN reagents (NAT and SIL) were purchased from Cambridge Isotope Laboratories (Tewksbury, MA). PNGase F was purchased from Bulldog Bio (Portsmouth, NH). Methanol, water, acetic acid, formic acid, and acetonitrile (Optima LC-MS grade) were purchased from Fisher Scientific (Hampton, NH). All reagents were used as received, unless otherwise specified.

Preparation of biological glycoprotein standards The glycoprotein standards, horseradish peroxidase and bovine fetuin, and human plasma samples were prepared using a modified FANGS procedure, as described previously [26, 40, 41]. Briefly, 250 μg of glycoprotein was added to a 10-kDa molecular weight cut-off filter. Glycoproteins were denatured using 2 μL of DTT diluted in 200 μL of 100 mM ammonium bicarbonate solution (digest buffer), vortexed briefly, and allowed to incubate at 56 °C for 30 min. Following incubation, the proteins were alkylated through the addition of 50 μL of 1 M iodoacetamide then incubated for 60 min at 37 °C. The denatured and alkylated proteins were concentrated on the filter using centrifugation for 40 min at 14,000 × g at 20 °C. The samples were subsequently washed in triplicate by first adding 100 μL of digest buffer to the filter, and then concentrated on the filter by centrifuging for 20 min. Prior to enzymatic separation of glycans from glycoproteins, the filters containing the washed glycoprotein samples were transferred to new, clean vials to prevent contamination during the collection of the cleaved glycans. Two microliters of PNGase F (1000 units) were added to each filter and subsequently diluted in 98 μL of digest buffer. Samples were mixed by aspirating on the filter, then incubated at 37 °C for 18 h. Following incubation, the released glycans were collected by centrifuging for 20 min at 14,000 × g. Samples were then washed in triplicate by adding 100 μL digest buffer followed by centrifugation at 14,000 × g for 20 min at 20 °C. After the washes were completed, the samples were incubated at − 80 °C until completely frozen, then subsequently dried to completion in a vacuum concentrator at 55 °C. Enzymatically released glycans were stored at − 20 °C until subsequent derivatization.

INLIGHT™ derivatization Prior to derivatization, glycan standards and maltoheptaose were reconstituted in LC-MS-grade water. Ten to 50 μg of each glycan standard or 50 μg of maltoheptaose were placed in a vacuum concentrator until completely dry. The enzymatically released glycans, 50 μg maltoheptaose, and 10–50 μg of the *N*-linked glycan standards were derivatized with natural (NAT)- and stable-isotope-labeled (SIL) INLIGHT™ reagents using a slight modification of a protocol that has been described previously [17]. The INLIGHT™ reagents were solubilized in 1 mL of LC-MS-grade methanol and vortexed for 10 min to ensure complete solubilization of the derivatization reagent, ensuring a final concentration of 1 mg/mL. Given the fundamental nature of these studies, both the NAT and SIL INLIGHT™ reagent were added to each sample in a 1:1 ratio at a concentration of 0.1 μg/μL prior to incubation to reduce analytical variability. The samples were then diluted in a solution of 45:55 (v:v) acetic acid:methanol. After briefly vortexing and centrifuging (ca. 5 s), the samples were allowed to incubate at 37 °C for 1.75 h. The derivatization reaction was quenched by drying the samples to completion in a vacuum concentrator at 55 °C. Derivatized glycans were stored at − 20 °C until analysis. The derivatized glycans were reconstituted in 50 μL of mobile phase A immediately prior to analysis.

nLC-IMS-MS analysis of INLIGHT™ derivatized glycans The nanoflow liquid chromatography (nLC) measurements were conducted using a Thermo Fisher Scientific EASY nLC 1200 (Waltham, MA) coupled with an Agilent 6560 IMS-QTOF (Santa Clara, CA). The RPLC separation of the derivatized glycans was performed using a Thermo Fisher Scientific (West Palm Beach, FL) Acclaim PepMap C18 analytical column (75 μm × 25 cm, 3 μm, 100 Å) preceded by a Thermo Scientific (West Palm Beach, FL) Acclaim PepMap C18 trap column (100 μm × 2 cm; 5 μm, 100 Å). Mobile phase A was comprised of 98% water, 2% acetonitrile, and 0.1% formic acid. Mobile phase B was comprised of 80% acetonitrile, 20% water, and 0.1% formic acid. The gradient used for RPLC began with 5% B, then increased to 35% over 2 min, then steadily ramped to 70% B over 40 min, sharply increased to 95% B over 1 min, held at 95% B for 6 min, then decreased over 1 min to 5% B at 300 nL/min. This mobile phase composition was held for 10 min, giving a total gradient length of 60 min per sample. Five microliters of sample was injected for each glycan analysis.

IMS-MS analysis of INLIGHT™ derivatized glycans DTIMS-MS measurements were conducted using an Agilent 6560 IMS-QTOF (Santa Clara, CA) instrument thoroughly characterized in previous publications [42, 43]. Briefly, ionization was

performed using the Agilent nanoESI source in positive ionization mode with a capillary voltage of 2100 V. DTIMS measurements were collected under a uniform electric field of 17.3 V/cm with nitrogen buffer gas at a constant pressure of 3.95 Torr. DTIMS data was acquired in a 4-bit multiplexing mode, with a trap fill time of 3.9 ms and release time of 100 μs. Mass analysis was conducted over an *m/z* range of 100–3200 *m/z*. Additional instrumental parameters are included in the Supplementary information (ESM Tables S1–S3).

Calculation of CCS values of INLIGHT™ derivatized glycans Multiplexed data files were de-multiplexed using the PNNL Pre-Processor (publically available from https://omics.pnl.gov/software/pnnl-preprocessor), then imported into Agilent MassHunter IM-MS Browser (version 10.0). CCS values for the INLIGHT™ derivatized glycans were calculated using the single-field method, as described previously [43]. Briefly, a mixture of compounds with known *m/z* values and well-characterized CCS values (Agilent tune mix) were analyzed under conditions identical to that used for the analysis of derivatized glycans. The measured drift times of these compounds were used to make a calibration curve converting drift time to CCS using a linear regression derived from the Mason-Schamp equation (Eq. 1) [43].

$$t_A = \frac{\beta}{z}\left[\frac{m_i}{m_\beta + m_i}\right]^{1/2} \mathrm{CCS} + t_{fix} \quad (1)$$

The CCS for the glycans were then calculated using the resulting linear regression and the measured drift times of the derivatized glycans.

For the high-resolution de-multiplexing (HRdm) study, each data file was de-multiplexed using the PNNL Pre-Processor as described above and previously detailed by May et al. [44]. Following initial de-multiplexing, feature finding was performed using the IM-MS Browser (parameters shown in ESM Figure S1). The resulting feature list was saved as a .csv within the same folder as the raw, multiplexed file and the de-multiplex file. Each was imported into the Agilent HRdm 1.0 software and processed using the medium processing mode available with a peak saturation threshold of 0.4.

Results and discussion

INLIGHT™ derivatized *N*-linked glycans drift time align

To assess the nLC-IMS-MS workflow for the analysis of *N*-linked glycans derivatized using the INLIGHT™ strategy, initially several *N*-linked glycan standards ($(GlcNAc)_2Man_5$, $(NeuNAc\text{-}Gal\text{-}GlcNAc)_3Man_3(GlcNAc)_2$, $(Gal\text{-}GlcNAc)_2Man_3(GlcNAc)_2$, $(GlcNAc)_2Man_9$, $(NeuNAc\text{-}Gal\text{-}GlcNAc)_2Man_3(Fuc)(GlcNAc)_2$, $GalGlcNAc_2Man_3GlcNAc_2$glycan, and $(GlcNAc)_2Man_3(Fuc)(GlcNAc)_2$ glycan) and maltoheptaose were studied. While maltoheptaose is not an *N*-linked glycan, this oligosaccharide is a reducing sugar and as a result is able to undergo the hydrazide chemistry necessary to affix the INLIGHT™ reagent [24]. Both the *N*-linked glycan standards and maltoheptaose were derivatized using a 1:1 mixture of the NAT and SIL reagents, then resuspended in MPA prior to analysis with nLC-IMS-MS [17]. As previously mentioned, glycans derivatized using the INLIGHT™ strategy display two distinctive isotopic distributions which is imparted by the use of both a NAT and $^{13}C_6$ SIL label, facilitating rapid data analysis and relative quantitation of labeled glycans. In this study, both the NAT and SIL forms of maltoheptaose and the *N*-linked glycan standards were detected (Fig. 1), and their resulting CCS values evaluated (see ESM Tables S4–S5 CCS). Maltoheptaose and its other related oligosaccharides were primarily observed as singly charged, protonated ions for both the NAT- and SIL-labeled oligosaccharides (Fig. 1a). The nested spectra of maltoheptaose in Fig. 1a illustrate both the drift time-aligned NAT- and SIL-labeled forms. All of the INLIGHT™ derivatized maltooligosaccharides were observed to have a single IMS peak in their drift spectra, with the exception of maltohexaose, which was observed to have two different IMS isomers or conformers (see ESM Figure S2). While the exact annotation of the two IMS peaks observed for the derivatized maltohexaose is unknown, it is possible that they are due to the flexibility of the joined glycans or differences in linkage connectivity, although it remains unclear as to why this was only observed with the hexamer. Additionally, it was observed that both the NAT and SIL tags had two conformers (data not shown). In order to assess the impact of this on LC-IMS-MS assessments of derivatized *N*-linked glycans, derivatized *N*-linked glycan standards were also assessed. Nested spectra for a representative *N*-linked glycan standard are shown in Fig. 1b. The INLIGHT™ derivatized *N*-linked glycans were observed primarily as doubly charged, protonated ions as shown by Fig. 1b, which illustrates the typical $[NAT+2H^+]^{2+}$ and $[SIL+2H^+]^{2+}$ isotopic distributions for the *N*-linked glycan standard $(GlcNAc)_2Man_3(Fuc)(GlcNAc)_2$. The monoisotopic peaks for the NAT- and SIL-labeled NGA2F were also observed to be 3.0101 *m/z* different, or a mass difference of 6.0202 Da, consistent with an INLIGHT™ derivatized glycan pair. It was observed that the drift spectra associated with this derivatized glycan pair primarily consisted of a single peak, with the maximum drift time corresponding to a CCS of 418.3 Å^2. A small shoulder at approximately 31 ms was also observed, which was less than 10% of the observed abundance of the main drift time distribution of this derivatized glycan. The source of this shoulder could not be discerned given our current instrumentation, but could be due to the presence of epimeric carbons at the reducing end,

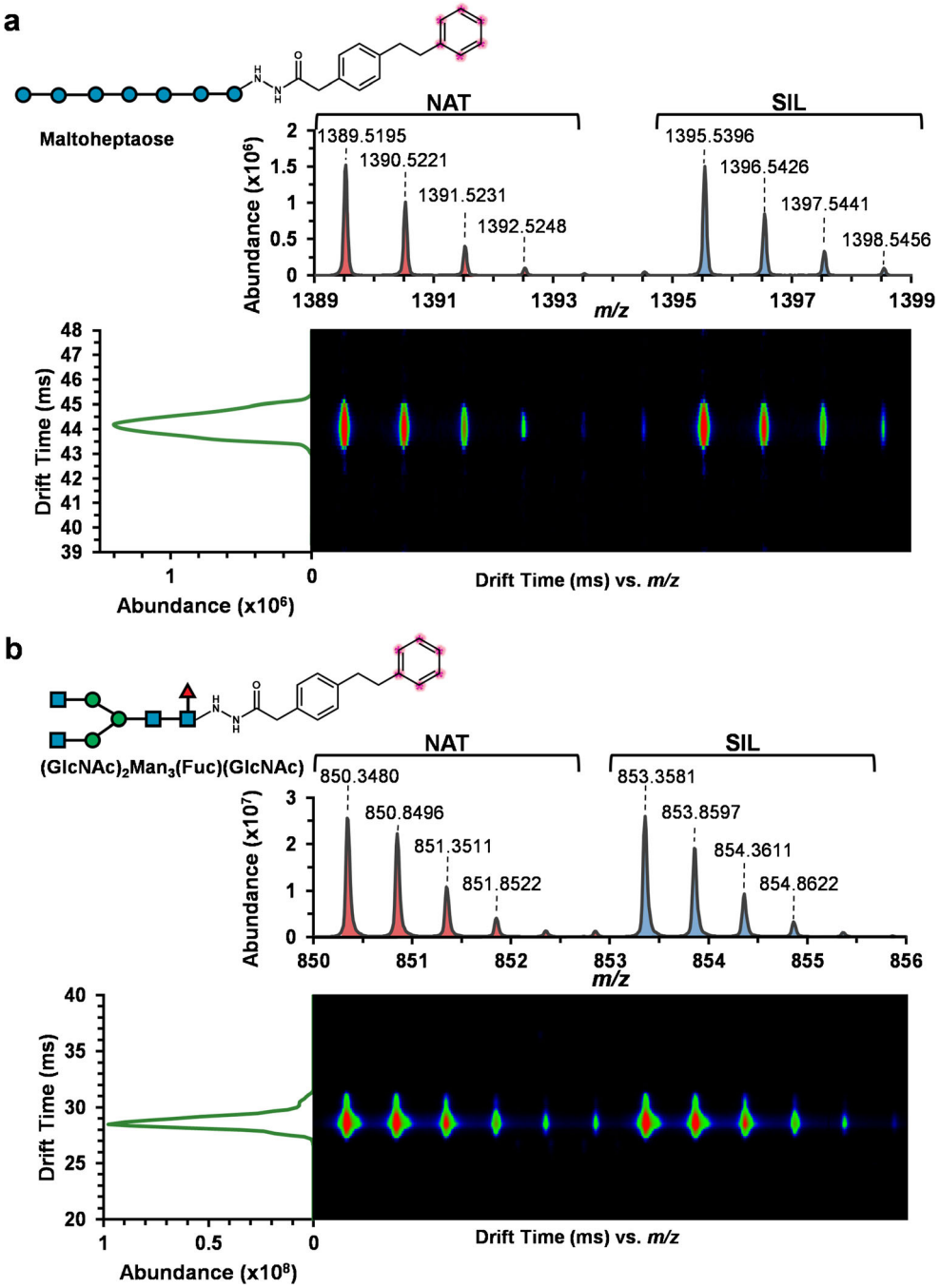

Fig. 1 The IMS-MS nested spectra for INLIGHT™ derivatized **a** maltoheptaose and **b** the *N*-linked glycan $(GlcNAc)_2Man_3(Fuc)(GlcNAc)_2$ standard, demonstrating isotopic distributions for both singly and doubly charged INLIGHT™ derivatized oligosaccharides. Glycans derivatized using the INLIGHT™ strategy are labeled using both a natural (NAT) and $^{13}C_6$ (denoted by asterisks) incorporated stable isotope label (SIL) reagent, and combined in a 1:1 ratio. This yields two distinctive isotopic distributions for each glycan. The incorporation of ^{13}C into the SIL also does not sufficiently change the structure of the molecule, resulting in drift time alignment of INLIGHT™ derivatized

the conformation of the INLIGHT™ reagent, or impurities within the glycan standard. The nested spectra shown in Fig. 1 also demonstrate that the NAT and SIL derivatized *N*-linked glycans have the same observed drift time, and thus, INLIGHT™ derivatized pairs are drift time-aligned. Consequently, the incorporation of a small number of $^{13}C_6$ within the SIL does not significantly change the glycan structure and results in drift time alignment for our measurements with a resolving power of ~ 60 at the 1+ charge state and slightly higher for the increasing charge states. As such, the pairwise drift time alignment and characteristic INLIGHT™ isotopic distributions can be used in the nLC-IMS-MS workflow to identify glycans in complex biological samples.

To assess the complementary nature of the INLIGHT™ strategy and the glycoprotein nLC-IMS-MS workflow, *N*-linked glycans from horseradish peroxidase and bovine fetuin were enzymatically cleaved using PNGase F, derivatized with INLIGHT™, and analyzed with nLC-IMS-MS. Since the

glycosylation of these two glycoproteins has been investigated thoroughly [45–47], they are ideal candidates as the resulting list of glycans previously identified could be curated and the corresponding INLIGHT™ derivatized NAT and SIL pairs determined. For our criteria, glycans were only considered identified if (1) both the NAT and SIL monoisotopic peaks were observed within the mass measurement error of the instrument (< 10 ppm); (2) the ratios of the NAT:SIL peaks were approximately 1:1; and (3) the NAT and SIL glycans were drift time-aligned as shown in Fig. 1. Using these criteria, four *N*-linked glycans were identified in horseradish peroxidase and twelve with bovine fetuin; CCS values were calculated for each (see ESM, Tables S6–S7).

The utility of IMS for removing noise and cleaning up MS spectra when interfaced within a standard LC-MS workflow has been previously demonstrated in both the fields of proteomics and glycomics [48–56]. In particular to glycomics, IMS filtering has been applied to the analysis of both native [54] and derivatized [56] glycans, and has even facilitated the analysis of glycans in complex matrices without additional sample clean-up [54, 57]. The IMS dimension was also found to be extremely helpful in removing noise from other ions in the present study. An example of this for INLIGHT™ derivatized *N*-linked glycans in complex samples is shown in Fig. 2a, which illustrates a portion of the nested spectra in which the protonated, singly charged NAT and SIL pair for $(Man)_3(GlcNAc)_2$ was anticipated from horseradish peroxidase but several interfering signals occurred within the same *m*/*z* space. Drift time filtering using only the area for the aligned pairs, however, removed the interfering signals and a clean distribution was observed as shown in Fig. 2b. The ability of IMS to parse these overlapping distributions into their individual components is extremely useful for complex samples and studies where relative quantitation is desired.

Conformational ordering of INLIGHT™ derivatized glycans

The compositional differences observed within various classes of biomolecules, both in the types of subunits comprising the molecules as well as their preferential arrangement, allow diverse classes of biomolecules to take on conformations in a relative order where the more sizable molecules, such as lipids and peptides, display a larger conformation for their mass relative to smaller biomolecules such as carbohydrates and oligonucleotides [58–60]. This conformational ordering of biomolecules has been observed in DTIMS-MS studies, where plots of *m*/*z* vs CCS yield trend lines used to classify molecules based on their biological role. To investigate the relationship between the *m*/*z* of INLIGHT™ derivatized glycans with their gas-phase conformation, *m*/*z* versus CCS plots were generated for the singly and doubly charged *N*-linked glycans from the glycoproteins and *N*-linked glycan standards, as well as the singly charged maltooligosaccharides (Fig. 3). The resulting trend lines for each series and their associated R^2 are shown on Fig. 3. Representative structures from each classification, along with their associated trend line, can be found in the ESM (see Figure S3). As can be seen in Fig. 3, the $[M+NAT+H^+]^+$ and $[M+SIL+H^+]^+$ maltooligosaccharides (teal diamonds, $y = 0.1168x + 167.32$) and the $[M+NAT+H^+]^+$ and $[M+SIL+H^+]^+$ derivatized *N*-linked glycans (green circles, $y = 0.1555x + 139.05$) illustrated distinct trend lines, different from previously reported underivatized oligosaccharides (red squares, $y = 0.2238x + 100.15$) [61]. Given that maltoheptaose and its related oligosaccharides are linear whereas *N*-linked glycans maintain a branched arrangement, the occurrence of two distinct lines for the *N*-linked glycans and maltoheptaose is expected [59]. It was also noted that a majority of the singly charged $[M+NAT+H^+]^+$ and $[M+SIL+H^+]^+$ glycans in this study contained mannose as their terminal monosaccharide. The conformational ordering of doubly charged INLIGHT™ derivatized glycans was also investigated for the $[M+NAT+2H^+]^{2+}$ and $[M+SIL+2H^+]^{2+}$ both from glycoproteins (orange circles, $y = 0.2138x + 235.69$) and commercially available *N*-linked glycan standards (grey squares, $y = 0.1987x + 252.29$). As shown in Fig. 3, the doubly charged derivatized glycans fell on a separate trend line from the singly charged glycans as anticipated since DTIMS separates based on size, shape, and charge [60]. However, in Fig. 3, the two separate sources (glycoprotein and glycan standards) of $[M+NAT+2H^+]^{2+}$ and $[M+SIL+2H^+]^{2+}$ *N*-linked glycans share the same trend line. The INLIGHT™ derivatized glycans were also compared to the same charge state and adduct of permethylated *N*-linked glycans previously reported in a CCS database (yellow triangles, $y = 0.2514x + 243.64$) [36]. The INLIGHT™ derivatized glycans and their permethylated counterparts of the same charge state followed distinct, separate trend lines, allowing the method of derivatization for the *N*-linked glycans to be readily discriminated.

The ability to further classify and subdivide molecular trend lines into series based on the monosaccharides present within the structure has previously been demonstrated using IMS-MS for both *N*-linked glycan fragments and intact glycans [36, 62]. Of particular relevance to this investigation, Glaskin et al. demonstrated this subclassification for permethylated *N*-linked glycans utilizing DTIMS-MS [36]. In this work, the permethylated glycans and glycopeptides obtained from trypsin-digested glycoproteins followed distinct molecular trend lines,

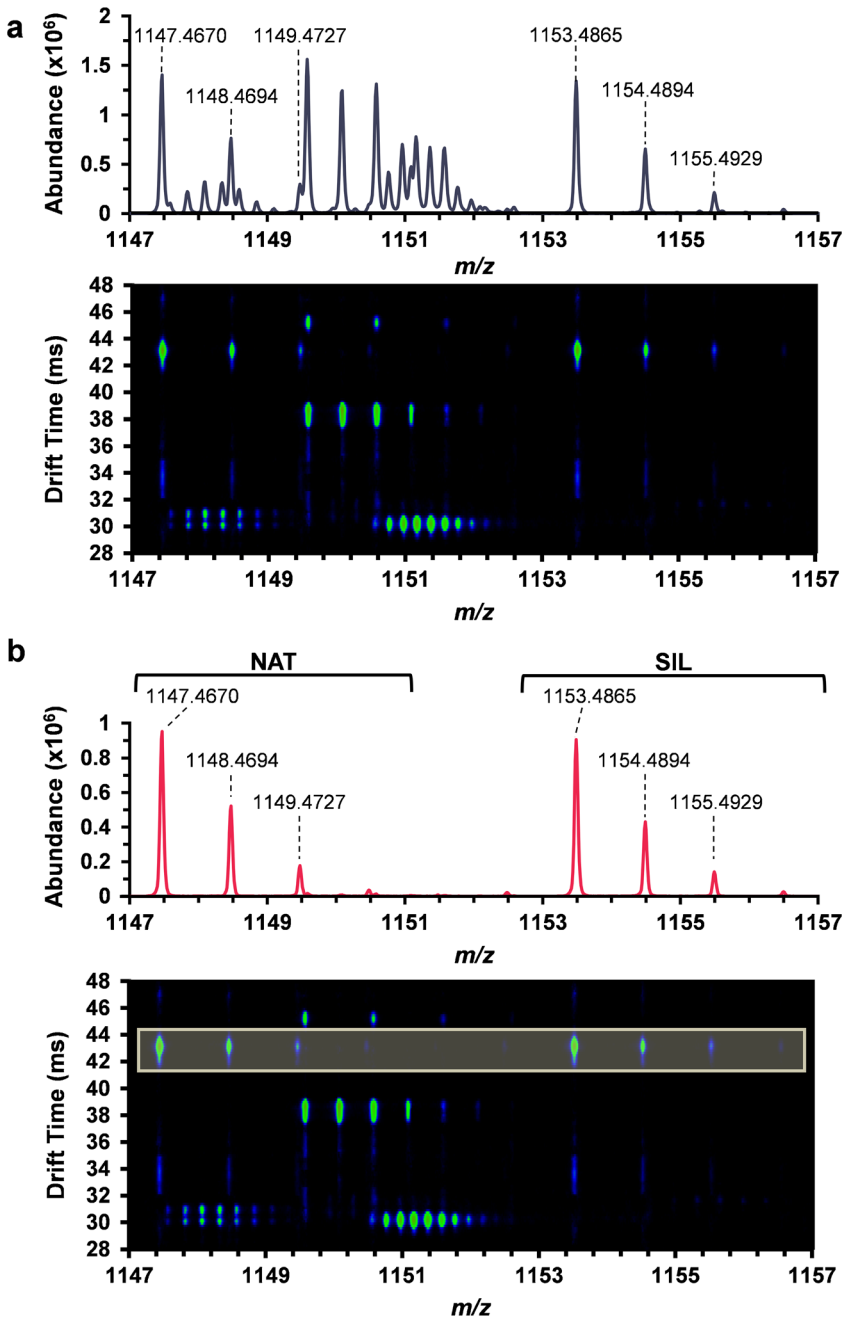

Fig. 2 IMS allows for the isolation of overlapping isotopic distributions, enabling the differentiation of glycans from other interfering signals. The IMS-MS nested spectra observed in **a** display overlapping isotopic distributions from multiple ions which obscure the confident identification of the INLIGHT™ derivatized glycan pair. **b** shows the nested spectra where the mass spectrum has been filtered by drift time, yielding a clean isotopic distribution for the NAT- and SIL-labeled *N*-linked glycan $(Man)_3(GlcNAc)_2$ in horseradish peroxidase

facilitating their analysis in complex biological samples [36]. They then investigated the ability of those molecular trend lines to subdivide both the glycopeptides and *N*-linked glycans based on the monosaccharides in their branched structures [36]. To investigate this potential relationship for INLIGHT™ glycans, the glycan standards and those derived from the glycoproteins horseradish peroxidase and bovine fetuin were subdivided based on the saccharide units located on their non-reducing end branches including terminal mannose (Fig. 4a), terminal galactose (Fig. 4b), and terminal sialic acid (Fig. 4c). Each subclassification was observed to fall along its own individual tend line (see ESM Figure S4a). It was observed that the INLIGHT™ glycans having a terminal mannose displayed a linear relationship between *m*/*z* and their associated CCS in both the 1+ and 2+ charge states (Fig. 4a), with both *m*/*z* and CCS increasing as the number of mannose within the *N*-glycan structure increased (see ESM Figure S4b). Linearity was also observed for those *N*-linked glycans containing a terminal galactose

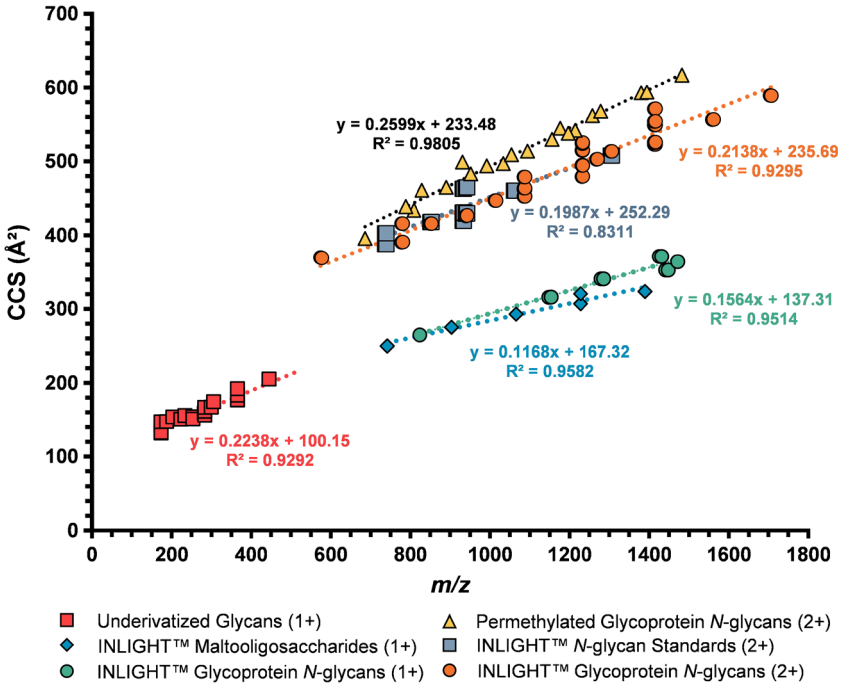

Fig. 3 CCS versus *m/z* trend lines for underivatized oligosaccharides (1+, red squares) [61], INLIGHT™ derivatized maltooligosaccharides (1+, teal diamonds), and both INLIGHT™ derivatized *N*-linked glycans from glycan standards (2+, grey squares) and those enzymatically released from the glycoprotein standards horseradish peroxidase and bovine fetuin (1+, green circles and 2+, orange circles). The 2+ charge state trend lines were compared with those observed for the permethylated *N*-linked glycan CCS database previously published by Glaskin et al. and shown in with yellow triangles [36]

(Fig. 4b) and was similarly found to be related to increasing numbers of galactose monosaccharides present (see ESM Figure S4c), but the linear relationship for those with terminal sialic acid was not as strong as the other classes (Fig. 4c). This was in part because many of the *N*-linked glycans observed within this subclass had multiple CCS values for the same *m/z* potentially indicating either the presence of isomeric species or the occurrence of multiple glycan conformers. Further investigations are needed to determine whether this is a function of structural

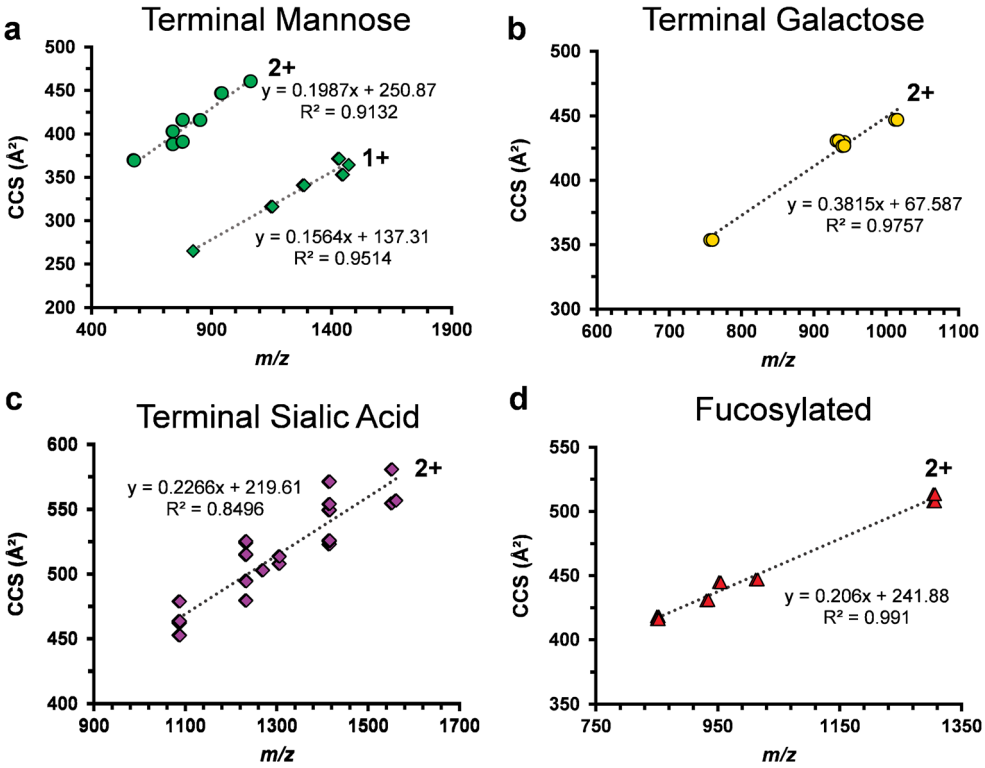

Fig. 4 CCS versus *m/z* plots for INLIGHT™ derivatized *N*-linked glycans from both glycan standards and enzymatically released from the glycoproteins horseradish peroxidase and bovine fetuin using PNGase F. *N*-linked glycans were grouped based on the terminal monosaccharides mannose (**a**), galactose (**b**), and sialic acid (**c**). Additionally, a trend line for glycans observed to be fucosylated was also noted (**d**)

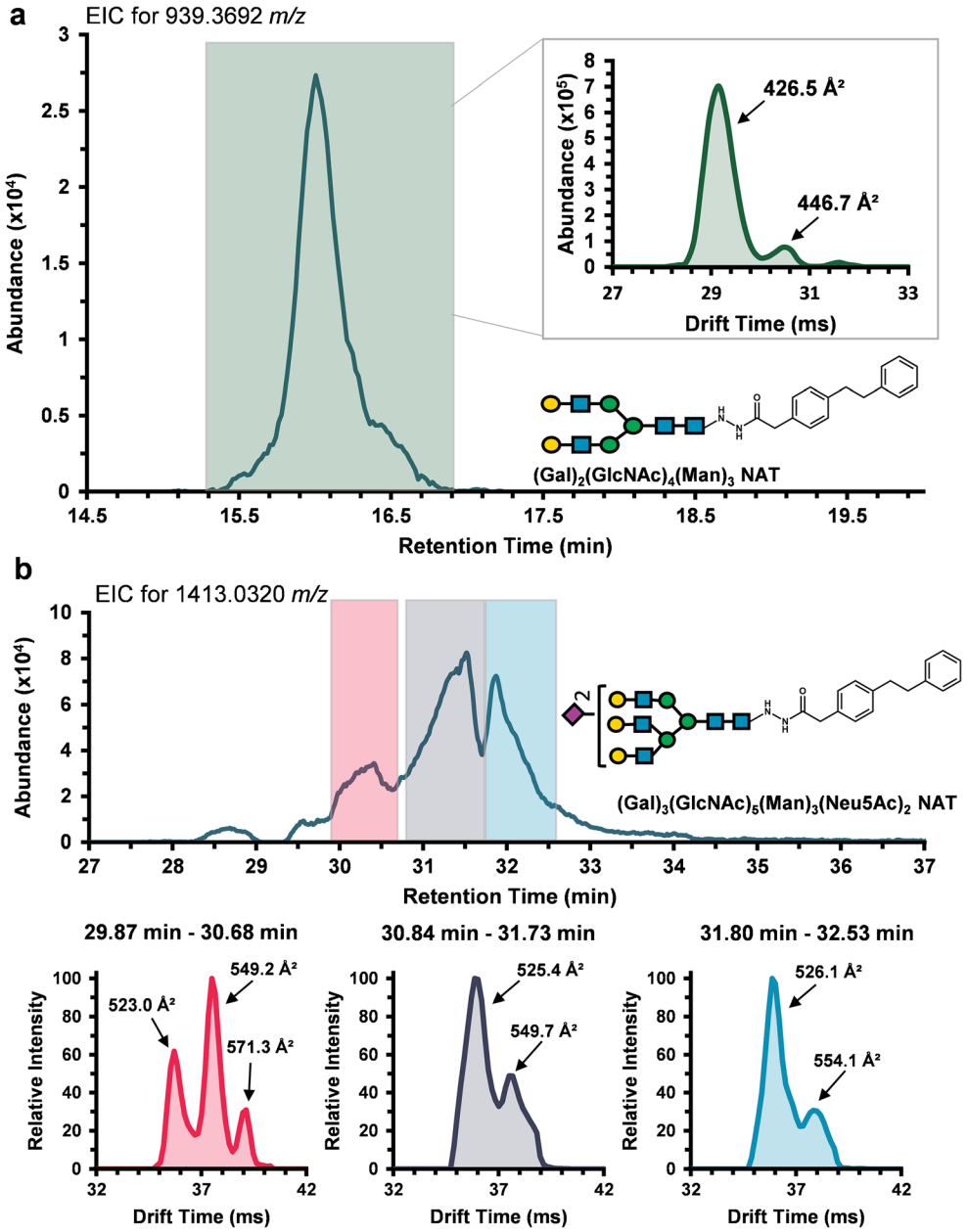

Fig. 5 The extracted ion chromatogram of the NAT-labeled *N*-linked glycan $(Fuc)_1(Gal)_2(GlcNAc)_4(Man)_3$ released from bovine fetuin (**a**) exhibited only one elution window. The inset shows the IMS drift time distribution associated with the *m*/*z* within the RT window highlighted by the green box. In contrast, an extracted ion chromatogram of the NAT-labeled *N*-linked glycan $(Gal)_3(GlcNAc)_5(Man)_3(Neu5Ac)_2$ released from bovine fetuin (**b**) illustrating multiple RT elution windows for the single *m*/*z* value. Examination of the drift time distribution within the labeled retention windows indicate multiple isomers are present in the different retention windows observed. The potential changes in glycan structure and conformation may explain the multiple retention windows observed for this single *m*/*z* but demonstrates the need for a deeper understanding of glycan structure and ultimately their function

differences within the glycans or actual changes in conformation. Additionally, all glycans that contained the monosaccharide fucose, regardless of the terminal monosaccharide unit, were observed to have a linear relationship between their *m*/*z* and corresponding CCS (Fig. 4d). We are currently investigating this trend as a way to analytically assign terminal monosaccharides.

nLC-IMS-MS *N*-linked glycan conformational landscape

Since IMS measurements occur on the millisecond timescale, they nest well within that of both LC separations (minutes) and time-of-flight MS assessments (microseconds) [63]. Furthermore, IMS allows for the

evaluation of co-eluting isomers that may not readily separate using LC analyses. In the present study, the majority of the glycans detected primarily eluted in a narrow elution window, as shown by the extracted ion chromatogram (EIC) for the NAT derivatized *N*-linked glycan $(Gal)_2(GlcNAc)_4(Man)_3$ from bovine fetuin (Fig. 5a). Two potential isomers/conformers were observed for this particular *m*/*z* (939.3692 *m*/z) within its retention window, as shown by the drift time distribution within the inset, with measured CCS of 426.5 $Å^2$ and 446.7 $Å^2$. However, a few of the INLIGHT™ derivatized *N*-linked glycans detected within the glycoprotein samples had multiple elution windows. An example is shown in Fig. 5b, which depicts the EIC for the NAT-labeled *N*-linked glycan $(Gal)_3(GlcNAc)_5(Man)_3(NeuAc)_2$ enzymatically released from bovine fetuin. This EIC showed three prominent chromatographic peaks. To assess the IMS conformation of the glycan within each retention window, the drift time distribution associated with 1413.0335 *m*/z in each LC window was extracted (Fig. 5b). The drift time distribution for the first LC window, 29.87 min to 30.68 min, showed at least three isomers with CCS values of 523.0 $Å^2$, 549.2 $Å^2$, and 571.3 $Å^2$ (with error below 0.4% RSD using triplicate measurements). The second LC window, 30.84 min to 31.73 min, had a distinctive change in the associated drift time distribution, showing at least two isomers with CCS values of 525.4 $Å^2$ and 549.7 $Å^2$. Again, the CCS values change in the third LC window showing at least two isomers present with CCS of 526.1 $Å^2$ and 554.1 $Å^2$. Thus, IMS illustrated multiple species in each LC elution window and demonstrates the vast structural complexity for these glycans which is beyond the scope of this study.

As stated previously, one of the limitations of this technique is the ability to discern information about structural or linkage isomers as opposed to changes in derivatized *N*-linked glycan conformation. Thus, the data shown in Fig. 5 was compared with previously published data in order to better understand the variability that we observe in our CCS measurements. Figure 5a, which depicts a narrow elution window for the glycan $(Gal)_2(GlcNAc)_4(Man)_3$ with two potential isomers/conformers. Previous investigations of this glycan using capillary electrophoresis and NMR indicated that approximately 90% of the observed galactose linkages for this glycan are in the β1–4 in all locations, while approximately 10% have a single branch with a β1–3 [64, 65]. While the current nLC-IMS-MS method currently precludes assignment of linkages, this lends evidence to the observation of two conformers/isomers within our bovine fetuin data for this specific glycan, particularly given that the two observed drift spectra peaks are in approximately the ratio previously reported in the literature. Previously published NMR data for bovine fetuin [65] has indicated that the tribranched, sialylated *N*-linked glycans comprise approximately 83% of the *N*-linked glycans within bovine fetuin. However, there is a high degree of complexity within this structure, ranging from the observation of β1–4 vs β1–3 linkages for the Gal moieties within the branches to the linkage type (α2–3 versus α2–6) and actual location of the Neu5Ac monosaccharides on the branched structures. When accounting for the location of the two Neu5Ac moieties alone, there are at least three possible isomers for this same *m*/z that have been previously reported [65]. Thus, while we are unable to assign structural and linkage isomers versus potential glycan conformers given our current findings, the observation of both multiple chromatographic windows combined with multiple apparent peaks within each corresponding drift spectra agrees with the high degree of chemical complexity associated with this *N*-linked glycan noted using other techniques.

Currently, one of the major limitations of many IMS platforms is the lack of resolving power possible for closely related structures. As structural changes between related glycan isomers may be subtle, the information obtained from drift time distributions alone may not be able to readily differentiate potential glycan isomers. As shown in Fig. 5b, there were some glycans observed that not only had multiple elution times, but also had broad drift time distributions indicative of additional isomers or conformers that could not be baseline separated within this drift tube. To investigate these broad distributions, the data shown in Fig. 5 was also analyzed using a high-resolution de-multiplexing (HRdm) approach previously demonstrated to improve the resolving power of the Agilent 6560 DTIMS-MS platform from ~ 60 to somewhere between 180 and 250 without compromising the associated CCS measurements [44]. This analysis strategy is employed post-acquisition, and consequently can be readily performed on any DTIMS-MS data files acquired with multiplexing.

To investigate the application of the HRdm algorithm for the analysis of the INLIGHT™ derivatized glycans, IMS-MS data for bovine fetuin (Fig. 5) was reprocessed using the HRdm 1.0 at its medium processing power. Currently, HRdm is available with three separate processing levels, each with a different average resolving power. To enhance the resolving power while minimizing both the potential for artifacts and the reduction of data points, the medium processing power was utilized here. The additional parameters used to process the glycan data were determined using Agilent tune mix files, also acquired with 4-bit multiplexing and de-multiplexed using the PNNL Pre-Processor. The ions from the tune mix display a single, unimodal drift time distribution with a highly characterized CCS value [43], so parameters were optimized to maintain this prior to application with more complex glycan data sets. Figure 6a illustrates the

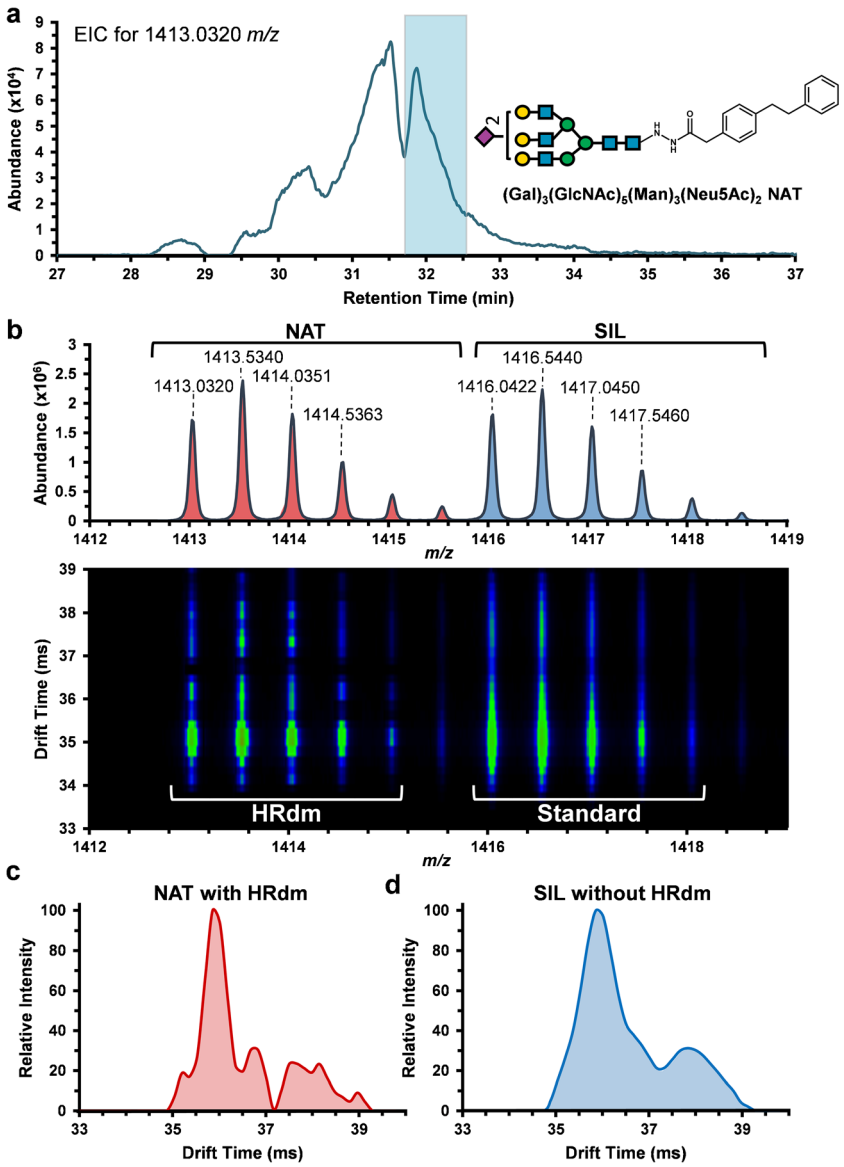

Fig. 6 To assess the HRdm algorithm analysis of INLIGHT™ derivatized N-linked glycans from bovine fetuin, the drift time distributions obtained within the third retention window of the *N*-linked glycan $(Gal)_3(GlcNAc)_5(Man)_3(NeuAc)_2$ was examined. **a** The NAT-labeled form was selected for HRdm analysis, as shown in the IMS nested spectra. The resulting drift time distribution (**b**) illustrated HRdm can be used to better resolve closely related derivatized isomers/conformers, as HRdm predicted at least six potential peaks (NAT with HRdm) within the drift time distribution (**c**) compared to the two observed without HRdm (**d**)

resulting IMS-MS nested spectra obtained for the third chromatographic window (31.80 min to 32.53 min) of the *N*-linked glycan $(Gal)_3(GlcNAc)_5(Man)_3(NeuAc)_2$. Since the NAT and SIL glycans are drift time-aligned and have identical drift time distributions prior to processing, suggesting that the incorporation of $^{13}C_6$ does not significantly alter the structure, HRdm was only performed on the NAT for direct comparison in the same nested spectra (Fig. 6b). Interestingly, the resulting nested spectra and drift time distribution after HRdm illustrate at least 6 peaks (Fig. 6c, d) as compared to the ~ 2 before. While the exact composition of the glycan structure cannot be assigned from this information alone, these data serve as a starting point for further investigations into glycan configuration utilizing this technique. Furthermore, it agrees well with the high degree of glycan structural complexity suggested by previous work using other analytical methods [64, 65].

Application of nLC-IMS-MS to INLIGHT™ derivatized glycans in complex samples

The nLC-IMS-MS analytical workflow was applied to enzymatically released *N*-linked glycans from pooled human plasma to assess its utility to define the glycans in a complex biological system. Pooled plasma has previously been assessed using INLIGHT™ on an Orbitrap™ mass spectrometer, and therefore, a target list exists from this study [26]. A representative base peak chromatogram (BPC) obtained for INLIGHT™ derivatized *N*-linked

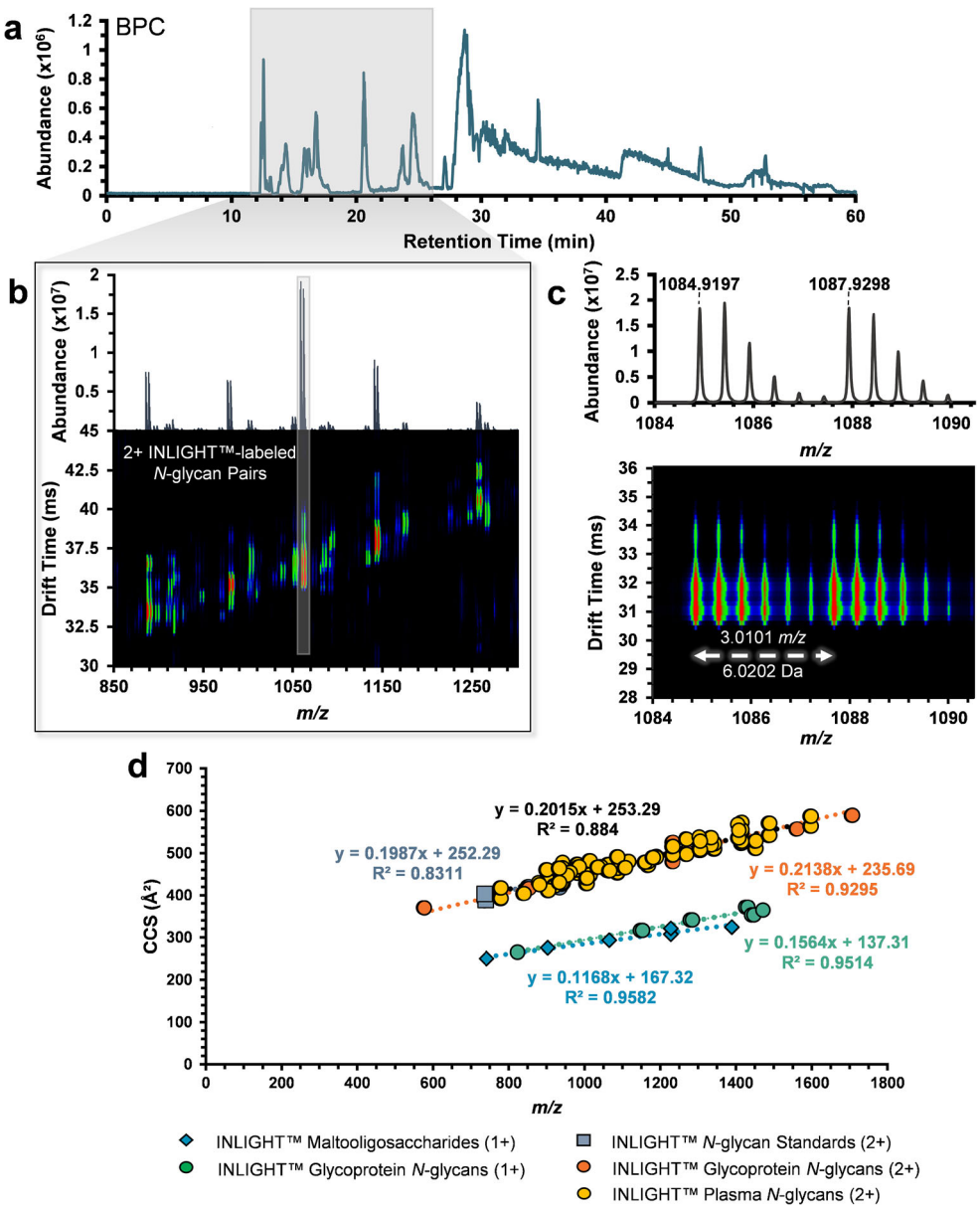

Fig. 7 The base peak chromatogram for the nLC-IMS-MS analysis of INLIGHT™ derivatized *N*-linked glycans enzymatically released from human pooled plasma (**a**). Many drift-aligned peak pairs were observed between 11 and 26 min in the LC gradient (**b**). A zoomed-in view of one selected drift-aligned pair (**c**) illustrates a separation of 3.0101 *m/z*, consistent with a 2+ INLIGHT™ derivatized *N*-glycan. The identified features from plasma that displayed the distinctive isotopic distribution of being NAT- and SIL-labeled in an approximate 1:1 ratio and were drift time-aligned were then plotted on the *m/z* vs. CCS trend lines established in Fig. 3 (**d**)

glycans from pooled human plasma is shown in Fig. 7a. It was observed that a majority of the INLIGHT™ derivatized *N*-linked glycans eluted between 11 and 26 min using the current nLC gradient (grey box in Fig. 7a). To show the benefit of IMS within a traditional nLC-MS workflow, the data was summed over this chromatographic window and the resulting IMS and MS nested spectra are shown in Fig. 7b. Numerous 2+ ion pairs that displayed the characteristic isotopic distribution for INLIGHT™ derivatized glycans were observed (Fig. 7b, c). To verify these pairs, their *m/z* was compared to the plasma INLIGHT™ derivatized *N*-glycan target list based on the work by Hecht et al. [26], resulting in the identification of 37 *N*-linked glycans in the pooled plasma samples (see ESM Table S8). After putative identification, each of the INLIGHT™ derivatized *N*-glycans from the pooled plasma was compared to the trend lines observed for the 1+ and 2+ INLIGHT™ derivatized *N*-glycans (Fig. 7d, yellow circles) established by both the derivatized *N*-linked glycan standards as well as those enzymatically released from the glycoproteins bovine fetuin and horseradish peroxidase (Fig. 3). These putative plasma *N*-linked glycans mapped onto the *m/z* vs CCS trend line observed for INLIGHT™ derivatized glycans within the same charge state (Fig. 3), providing increased confidence in these identifications. This approach is particularly advantageous for analysis of *N*-glycans from complex biological samples that have not been previously

characterized as the paired features observed within nLC-IMS-MS data facilitate more confident identifications beyond those obtained using nLC-MS alone.

Conclusions

The combination of nLC-IMS-MS and the INLIGHT™ provides a rapid analysis strategy for *N*-glycans in complex samples. The use of IMS drift time alignment for the NAT- and SIL-labeled *N*-glycans, combined with the distinctive isotopic distributions provided by the incorporation of the $^{13}C_6$, facilitates confident identifications of *N*-linked glycans within complex biological samples. Additionally, as the INLIGHT™ labeled glycans appear to have molecular trend lines based on *m*/*z* and CCS values, as has previously been observed in IMS for other classes of biologically relevant molecules, the rapid identification of putative glycans and glycan subclasses is possible. This ability lends itself well to the analysis of novel sample types for which there is no literature precedence for the *N*-linked glycans being observed. While further investigations into linkage assignments are still necessary, these experimental findings can be used with fragmentation data and computational investigations for putative annotations of glycan structures.

Supplementary Information The online version contains supplementary material available at https://doi.org/10.1007/s00216-021-03570-7.

Acknowledgements The ion mobility spectrometry-mass spectrometry measurements were carried out in the Molecular Education, Technology and Research Innovation Center (METRIC) at North Carolina State University. The authors gratefully acknowledge the financial support received from the NIH National Institute on Aging (R56 AG063885), NIH National Institute of Environmental Health Sciences (P30 ES025128) and North Carolina State University.

Declarations None of the authors report any conflicts of interest.

References

1. Lin B, Qing X, Liao J, Zhuo K. Role of protein glycosylation in host-pathogen interaction. Cells. 2020;9(4):1022.
2. Alter G, Ottenhoff THM, Joosten SA. Antibody glycosylation in inflammation, disease and vaccination. Semin Immunol. 2018;39:102–10.
3. Varki A, Gagneux P. (2015) Biological functions of glycans. In: Varki A, Cummings RD, Esko JD, Stanley P, Hart GW, Aebi M, et al., editors. Essentials of glycobiology. Cold Spring Harbor (NY)p. 77-88.
4. Molinari M. N-glycan structure dictates extension of protein folding or onset of disposal. Nat Chem Biol. 2007;3(6):313–20.
5. Tarentino AL, Gomez CM, Plummer TH. Deglycosylation of asparagine-linked glycans by peptide:N-glycosidase F. Biochemistry. 1985;24(17):4665–71.
6. (2015) In: Varki A, Cummings RD, Esko JD, Stanley P, Hart GW, Aebi M, et al., editors. Essentials of glycobiology. Cold Spring Harbor (NY)
7. Stanley P, Taniguchi N, Aebi M. (2015). N-Glycans. In: Varki A, Cummings RD, Esko JD, Stanley P, Hart GW, Aebi M, et al., editors. Essentials of glycobiology. Cold Spring Harbor (NY)p. 99-111.
8. Videira PAQ, Castro-Caldas M. Linking glycation and glycosylation with inflammation and mitochondrial dysfunction in Parkinson's disease. Front Neurosci. 2018;12:381.
9. Schedin-Weiss S, Winblad B, Tjernberg LO. The role of protein glycosylation in Alzheimer disease. FEBS J. 2014;281(1):46–62.
10. Montefiori DC, Robinson WE Jr, Mitchell WM. Role of protein N-glycosylation in pathogenesis of human immunodeficiency virus type 1. Proc Natl Acad Sci U S A. 1988;85(23):9248–52.
11. Pinho SS, Reis CA. Glycosylation in cancer: mechanisms and clinical implications. Nat Rev Cancer. 2015;15(9):540–55.
12. Laine RA. A calculation of all possible oligosaccharide isomers both branched and linear yields 1.05 x 10(12) structures for a reducing hexasaccharide: the isomer barrier to development of single-method saccharide sequencing or synthesis systems. Glycobiology. 1994;4(6):759–67.
13. Mulloy B, Dell A, Stanley P, Prestegard JH. (2015) Structural analysis of glycans. In: Varki A, Cummings RD, Esko JD, Stanley P, Hart GW, Aebi M, et al., editors. Essentials of glycobiology. Cold Spring Harbor (NY). p. 639-52.
14. Abrahams JL, Campbell MP, Packer NH. Building a PGC-LC-MS N-glycan retention library and elution mapping resource. Glycoconj J. 2018;35(1):15–29.
15. Ashwood C, Pratt B, MacLean BX, Gundry RL, Packer NH. Standardization of PGC-LC-MS-based glycomics for sample specific glycotyping. Analyst. 2019;144(11):3601–12.
16. Walker SH, Lilley LM, Enamorado MF, Comins DL, Muddiman DC. Hydrophobic derivatization of N-linked glycans for increased ion abundance in electrospray ionization mass spectrometry. J Am Soc Mass Spectrom. 2011;22(8):1309–17.
17. Kalmar JG, Butler KE, Baker ES, Muddiman DC. Enhanced protocol for quantitative N-linked glycomics analysis using Individuality Normalization when Labeling with Isotopic Glycan Hydrazide Tags (INLIGHT)™. Anal Bioanal Chem. 2020;412(27):7569–79.
18. Ruhaak LR, Zauner G, Huhn C, Bruggink C, Deelder AM, Wuhrer M. Glycan labeling strategies and their use in identification and quantification. Anal Bioanal Chem. 2010;397(8):3457–81.
19. Ritamo I, Räbinä J, Natunen S, Valmu L. Nanoscale reversed-phase liquid chromatography-mass spectrometry of permethylated N-glycans. Anal Bioanal Chem. 2013;405(8):2469–80.
20. Shajahan A, Supekar NT, Heiss C, Ishihara M, Azadi P. Tool for rapid analysis of glycopeptide by permethylation via one-pot site mapping and glycan analysis. Anal Chem. 2017;89(20):10734–43.
21. Keser T, Pavić T, Lauc G, Gornik O. Comparison of 2-aminobenzamide, procainamide and RapiFluor-MS as derivatizing agents for high-throughput HILIC-UPLC-FLR-MS N-glycan analysis. Front Chem. 2018;6:324.
22. Hahne H, Neubert P, Kuhn K, Etienne C, Bomgarden R, Rogers JC, et al. Carbonyl-reactive tandem mass tags for the proteome-wide quantification of N-linked glycans. Anal Chem. 2012;84(8):3716–24.
23. Walker SH, Taylor AD, Muddiman DC. Individuality Normalization when Labeling with Isotopic Glycan Hydrazide Tags (INLIGHT): a novel glycan-relative quantification strategy. J Am Soc Mass Spectrom. 2013;24(9):1376–84.
24. Walker SH, Budhathoki-Uprety J, Novak BM, Muddiman DC. Stable-isotope labeled hydrophobic hydrazide reagents for the

relative quantification of N-linked glycans by electrospray ionization mass spectrometry. Anal Chem. 2011;83(17):6738–45.
25. Hecht ES, Scholl EH, Walker SH, Taylor AD, Cliby WA, Motsinger-Reif AA, et al. Relative quantification and higher-order modeling of the plasma glycan cancer burden ratio in ovarian cancer case-control samples. J Proteome Res. 2015;14(10):4394–401.
26. Hecht ES, McCord JP, Muddiman DC. Definitive screening design optimization of mass spectrometry parameters for sensitive comparison of filter and solid phase extraction purified, INLIGHT plasma N-glycans. Anal Chem. 2015;87(14):7305–12.
27. Loziuk PL, Hecht ES, Muddiman DC. N-linked glycosite profiling and use of Skyline as a platform for characterization and relative quantification of glycans in differentiating xylem of *Populus trichocarpa*. Anal Bioanal Chem. 2017;409(2):487–97.
28. Manz C, Pagel K. Glycan analysis by ion mobility-mass spectrometry and gas-phase spectroscopy. Curr Opin Chem Biol. 2018;42:16–24.
29. Mu Y, Schulz BL, Ferro V. Applications of ion mobility-mass spectrometry in carbohydrate chemistry and glycobiology. Molecules. 2018;23(10):2557.
30. Both P, Green AP, Gray CJ, Sardzík R, Voglmeir J, Fontana C, et al. Discrimination of epimeric glycans and glycopeptides using IM-MS and its potential for carbohydrate sequencing. Nat Chem. 2014;6(1):65–74.
31. Plasencia MD, Isailovic D, Merenbloom SI, Mechref Y, Novotny MV, Clemmer DE. Resolving and assigning N-linked glycan structural isomers from ovalbumin by IMS-MS. J Am Soc Mass Spectrom. 2008;19(11):1706–15.
32. Isailovic D, Kurulugama RT, Plasencia MD, Stokes ST, Kyselova Z, Goldman R, et al. Profiling of human serum glycans associated with liver cancer and cirrhosis by IMS−MS. J Proteome Res. 2008;7(3):1109–17.
33. Zheng X, Zhang X, Schocker NS, Renslow RS, Orton DJ, Khamsi J, et al. Enhancing glycan isomer separations with metal ions and positive and negative polarity ion mobility spectrometry-mass spectrometry analyses. Anal Bioanal Chem. 2017;409(2):467–76.
34. Fenn LS, McLean JA. Structural resolution of carbohydrate positional and structural isomers based on gas-phase ion mobility-mass spectrometry. Phys Chem Chem Phys. 2011;13(6):2196–205.
35. Morrison KA, Bendiak BK, Clowers BH. Assessment of dimeric metal-glycan adducts via isotopic labeling and ion mobility-mass spectrometry. J Am Soc Mass Spectrom. 2018;29(8):1638–49.
36. Glaskin RS, Khatri K, Wang Q, Zaia J, Costello CE. Construction of a database of collision cross section values for glycopeptides, glycans, and peptides determined by IM-MS. Anal Chem. 2017;89(8):4452–60.
37. Jooß K, Meckelmann SW, Klein J, Schmitz OJ, Neusüß C. Capillary zone electrophoresis coupled to drift tube ion mobility-mass spectrometry for the analysis of native and APTS-labeled N-glycans. Anal Bioanal Chem. 2019;411(24):6255–64.
38. Mason EA, Schamp HW. Mobility of gaseous lons in weak electric fields. Ann Phys. 1958;4(3):233–70.
39. Revercomb HE, Mason EA. Theory of plasma chromatography/gaseous electrophoresis. Rev Anal Chem. 1975;47(7):970–83.
40. Abdul Rahman S, Bergström E, Watson CJ, Wilson KM, Ashford DA, Thomas JR, et al. Filter-aided N-glycan separation (FANGS): a convenient sample preparation method for mass spectrometric N-glycan profiling. J Proteome Res. 2014;13(3):1167–76.
41. Hecht ES, McCord JP, Muddiman DC. A quantitative glycomics and proteomics combined purification strategy. JoVE. 2016;109:e53735.
42. May JC, Jurneczko E, Stow SM, Kratochvil I, Kalkhof S, McLean JA. Conformational landscapes of ubiquitin, cytochrome c, and myoglobin: Uniform field ion mobility measurements in helium and nitrogen drift gas. Int J Mass Spectrom. 2018;427:79–90.
43. Stow SM, Causon TJ, Zheng X, Kurulugama RT, Mairinger T, May JC, et al. An interlaboratory evaluation of drift tube ion mobility–mass spectrometry collision cross section measurements. Anal Chem. 2017;89(17):9048–55.
44. May JC, Knochenmuss R, Fjeldsted JC, McLean JA. Resolution of isomeric mixtures in ion mobility using a combined demultiplexing and peak deconvolution technique. Anal Chem. 2020;92(14):9482–92.
45. Gray JSS, Yang BY, Montgomery R. Heterogeneity of glycans at each N-glycosylation site of horseradish peroxidase. Carbohydr Res. 1998;311(1):61–9.
46. Sun X, Tao L, Yi L, Ouyang Y, Xu N, Li D, et al. N-glycans released from glycoproteins using a commercial kit and comprehensively analyzed with a hypothetical database. J Pharm Anal. 2017;7(2):87–94.
47. Yang BY, Gray JSS, Montgomery R. The glycans of horseradish peroxidase. Carbohydr Res. 1996;287(2):203–12.
48. Baker ES, Burnum-Johnson KE, Ibrahim YM, Orton DJ, Monroe ME, Kelly RT, et al. Enhancing bottom-up and top-down proteomic measurements with ion mobility separations. Proteomics. 2015;15(16):2766–76.
49. Baker ES, Livesay EA, Orton DJ, Moore RJ, Danielson WF 3rd, Prior DC, et al. An LC-IMS-MS platform providing increased dynamic range for high-throughput proteomic studies. J Proteome Res. 2010;9(2):997–1006.
50. MacLean BX, Pratt BS, Egertson JD, MacCoss MJ, Smith RD, Baker ES. Using Skyline to analyze data-containing liquid chromatography, ion mobility spectrometry, and mass spectrometry dimensions. J Am Soc Mass Spectrom. 2018;29(11):2182–8.
51. Crowell KL, Slysz GW, Baker ES, LaMarche BL, Monroe ME, Ibrahim YM, et al. LC-IMS-MS Feature Finder: detecting multidimensional liquid chromatography, ion mobility and mass spectrometry features in complex datasets. Bioinformatics. 2013;29(21):2804–5.
52. Tang K, Li F, Shvartsburg AA, Strittmatter EF, Smith RD. Two-dimensional gas-phase separations coupled to mass spectrometry for analysis of complex mixtures. Anal Chem. 2005;77(19):6381–8.
53. Venne K, Bonneil E, Eng K, Thibault P. Improvement in peptide detection for proteomics analyses using nanoLC−MS and high-field asymmetry waveform ion mobility mass spectrometry. Anal Chem. 2005;77(7):2176–86.
54. Harvey DJ, Sobott F, Crispin M, Wrobel A, Bonomelli C, Vasiljevic S, et al. Ion mobility mass spectrometry for extracting spectra of N-glycans directly from incubation mixtures following glycan release: application to glycans from engineered glycoforms of intact, folded HIV gp120. J Am Soc Mass Spectrom. 2011;22(3):568–81.
55. Gray CJ, Thomas B, Upton R, Migas LG, Eyers CE, Barran PE, et al. Applications of ion mobility mass spectrometry for high throughput, high resolution glycan analysis. Biochim Biophys Acta Gen Subj. 2016;1860(8):1688–709.
56. Fenn LS, McLean JA. Enhanced carbohydrate structural selectivity in ion mobility-mass spectrometry analyses by boronic acid derivatization. Chem Commun. 2008;43:5505–7.
57. Harvey DJ, Crispin M, Bonomelli C, Scrivens JH. Ion mobility mass spectrometry for ion recovery and clean-up of MS and MS/MS spectra obtained from low abundance viral samples. J Am Soc Mass Spectrom. 2015;26(10):1754–67.
58. Fenn LS, McLean JA. Biomolecular structural separations by ion mobility–mass spectrometry. Anal Bioanal Chem. 2008;391(3):905–9.
59. McLean JA. The mass-mobility correlation redux: the conformational landscape of anhydrous biomolecules. J Am Soc Mass Spectrom. 2009;20(10):1775–81.
60. May JC, Goodwin CR, Lareau NM, Leaptrot KL, Morris CB, Kurulugama RT, et al. Conformational ordering of biomolecules in the gas phase: nitrogen collision cross sections measured on a

prototype high resolution drift tube ion mobility-mass spectrometer. Anal Chem. 2014;86(4):2107–16.
61. Zheng X, Aly NA, Zhou Y, Dupuis KT, Bilbao A, Paurus Vanessa L, et al. A structural examination and collision cross section database for over 500 metabolites and xenobiotics using drift tube ion mobility spectrometry. Chem Sci. 2017;8(11):7724–36.
62. Harvey DJ, Scarff CA, Edgeworth M, Pagel K, Thalassinos K, Struwe WB, et al. Travelling-wave ion mobility mass spectrometry and negative ion fragmentation of hybrid and complex N-glycans. J Mass Spectrom. 2016;51(11):1064–79.
63. May JC, McLean JA. Ion mobility-mass spectrometry: time-dispersive instrumentation. Anal Chem. 2015;87(3):1422–36.
64. Klamer Z, Hsueh P, Ayala-Talavera D, Haab B. Deciphering protein glycosylation by computational integration of on-chip profiling, glycan-array data, and mass spectrometry*[S]. Mol Cell Proteomics. 2019;18(1):28–40.
65. Green ED, Adelt G, Baenziger JU, Wilson S, Van Halbeek H. The asparagine-linked oligosaccharides on bovine fetuin. Structural analysis of N-glycanase-released oligosaccharides by 500-megahertz 1H NMR spectroscopy. J Biol Chem. 1988;263(34):18253–68.